Next Nanotechnology 5 (2024) 100038

Contents lists available at ScienceDirect

Next Nanotechnology

journal homepage: www.sciencedirect.com/journal/next-nanotechnology

Research article

Influence of annealing temperature on microstructure and phase transformations of oxide system Bi_2O_3/TiO_2 formed in aqueous solutions

Gennady Gorokh [a,*], Uladzimir Fiadosenka [a], Xiaozhi Wang [b], Igor Taratyn [c]

[a] Belarusian State University of Informatics and Radioelectronics, Minsk 220013, Belarus
[b] Zhejiang University, Hangzhou City 310000, PR China
[c] Belarusian National Technical University, Minsk 220013, Belarus

ARTICLE INFO

Keywords:
$Bi_4Ti_3O_{12}$ compound
Microstructure phase transformations
Successive ionic layer deposition
Annealing

ABSTRACT

Bismuth titanate is widely used in various fields of science and technology due to its unique physical and chemical properties. Nanostructured metal oxide compounds of the Bi–Ti–O system, consisting of columnar TiO_2 nanostructures obtained by electrochemical anodization of a two-layer Ti/Al composition, and platelet Bi_2O_3 nanostructures formed by sequential ion-layer deposition were synthesized. Morphological changes and phase transformations in the microstructure of the Bi_2O_3/TiO_2 oxide system, which occur during its thermal annealing at temperatures of 150, 300, 500, and 700 °C, have been studied. Annealing of the oxide system in the range of 150–300 °C degrees leads to inconsequential morphological and structural changes: the mixture of oxides is densified, in addition to anatase, a rutile phase appears in TiO_2. The crystal system of the Bi_2O_3 phase is hexagonal. After annealing at 500 °C, not only morphological changes occurred in the studied composite, but also significant transformations in the microstructure. In the film volume, oxide phases Ti_2O_3 and Bi_2O_3 began to transform into three-component compound $Bi_4Ti_3O_{12}$, and this process is completed at 700 degrees with the formation of single-phase $Bi_4Ti_3O_{12}$ nanocomposite with an orthorhombic lattice with the crystal space group *Fmmm*.

1. Introduction

Bismuth titanate is the best-known compound of Bi—Ti—O system, and widely used in acoustic, opto- and microelectronics, in particular, in capacitors, converters, non-volatile memory elements, piezoelectric sensors [1–3] due to its high piezoelectric and electrophysical properties [4]. Another equally important field of application of bismuth and titanium compounds is the treatment of wastewater from toxic organic pollutants that are not biodegradable [5,6]. Technology based on photocatalysis during the decomposition of carcinogens in sunlight is the most promising [7–9]. Bismuth titanate, due to its unique layered crystal structure and electronic band structure, effectively separates photogenerated electron–hole pairs [10,11] and exhibits pronounced photocatalytic activity in the decomposition of organic pollutants [12–16].

Bismuth titanate surfaces, in addition to their ability to generate electrons and holes, also easily adsorb molecules of gaseous medium, which opens up prospects for its use as a gas-sensitive material [17,18]. As a result of interaction with the surface, the adsorbed molecules give some of their energy to surface atoms and create local energy levels in the band gap, which are new surface centers that capture free charge carriers [19,20]. In the presence of a large amount of free charge carriers in bismuth titanate, adsorbed molecules on its surface lead to a change in electrical conductivity [21]. The mechanisms of catalytic action and the role of free electrons and holes in chemical reactions on the surface of metal oxide semiconductors are quite similar [22,23]. At the same time, due to the high specific area and small particle sizes, more active centers are created on the structured surface, which significantly affect the formation of electron pairs and holes and their efficient separation, which explains why nanostructured $Bi_4Ti_3O_{12}$ has better photocatalytic and gas-sensitive characteristics compared to smooth films of the same composition [24,25]. The use of nanostructured materials makes it possible to obtain a large area of the sensitive layer active surface [26]. Given the fact that sorption reactions occur mainly on the surface of the sensitive layer, the size of the semiconductor particles will have a significant effect on the sensor sensitivity. A method based on the deposition of different compositions materials on nanoporous anodic alumina (AA) matrices has become widespread for the formation of low-dimensional structures arrays and nanostructured films [27–29].

* Corresponding author.
E-mail addresses: gorokh@bsuir.by (G. Gorokh), xiaozhiwang@zju.edu.cn (X. Wang), mnt@bntu.by (I. Taratyn).

https://doi.org/10.1016/j.nxnano.2023.100038
Received 6 September 2023; Received in revised form 9 November 2023; Accepted 23 December 2023
Available online 2 January 2024

Vacuum methods [30,31], electrochemical [32,33], and chemical methods from the liquid phase [34,35] are used as deposition methods. One of the most promising chemical methods for the formation of thin films with various compositions is the successive ionic layer deposition (SILD) [36,37]. The SILD method is based on cycle treatment of substrates in solutions of ion-containing metal salts such as chlorides, nitrates, acetates. Another option for creating matrices of low-dimensional structures is anodizing layers of valve metals (Ti, Nb, Zr) through AA pores [38,39]; as a result, metal oxide nanostructures of a specific shape (mounds, columns, islands, etc.) are formed under the mask. The composition and properties of nanostructures are primarily determined by the conditions of electrochemical and thermal treatment. It is possible to controllably create nanostructures arrays of different sizes and various shapes by changing the metals of the sublayer, its thickness, the electrochemical conditions for anodizing aluminum, as well as the sublayer reanodization voltage [38,40]. Metal oxide nanostructures of the listed metals have their own specific properties, but titanium oxide islands or columns stand out among them, in which the oxide in various oxide phases from the Ti–O system predominates [41]. In this case, the stoichiometric oxide phases of titanium are located near the top of the island, and the stoichiometric composition of the oxide is more and more disturbed from the top to the bottom of the column.

In this work, we propose a new technological approach for the synthesis of compounds of the Bi–Ti–O system using liquid chemistry methods—electrochemical anodizing of two-layer Al/Ti system and the successive ionic layer deposition of bismuth oxide from aqueous solutions onto the formed matrix of the titanium metaloxide columns. The research of the microstructure and composition of the formed system and as phase transformations in high-temperature annealing are presented.

2. Materials and methods

Silicon substrates were used as initial samples, on which Ti (99,95 %) – 200 nm (bottom) and Al (99,999 %) – 1.5 μm were deposited by magnetron sputtering in vacuum. Electrochemical anodizing of experimental samples was carried out in a combined mode. The upper aluminum layer was anodized in an aqueous solution in 0.4 M H_3PO_4 (87 %, purissimum) in the potentiostatic mode at 150 V. As a result, the upper aluminum layer was transformed into a matrix with hexagonally packed oxide cells with vertical pores in the center.

The subsequent anodization of the titanium sublayer through the AA pores was carried out in aqueous solution of 0.2 M $C_4H_6O_6$ (99,9 %, purissimum speciale) at 250 V. On the second anodization stage, the nanosized columns of titanium oxide were formed under the AA pores and partially filled the lower part of the pores (Fig. 1a). The electrical anodizing modes were set using a Keysight N5752A system DC power supply, and the process parameters were recorded and monitored in situ using a Keysight 34470 A digital multimeter connected via a USB interface to a personal computer with the Bench Vue software installed. After reanodization, the AA mask was removed in 50 % H_3PO_4 (87 %, purissimum speciale) aqueous solution at temperature of 323 K.

The bismuth oxide layer was deposited on the formed titanium metal oxide columnar film using SILD method from the cationic aqueous solution of 0.1 M $Bi(NO_3)_3 \times 5\ H_2O$ (99,0 %, pro analysi) and the anionic solution – distilled water heated to 70 °C. After 150 cycles, the matrices with the formed composite films were annealed in an atmosphere of purified air at temperatures of 150, 300, 500, and 700 °C for 1.5 h.

The surface morphology of the formed films was studied by scanning electron microscopy (*SEM*) in Hitachi S-806 at accelerating voltage of 7 kV and Hitachi S4–800 at accelerating voltage of 15 kV.

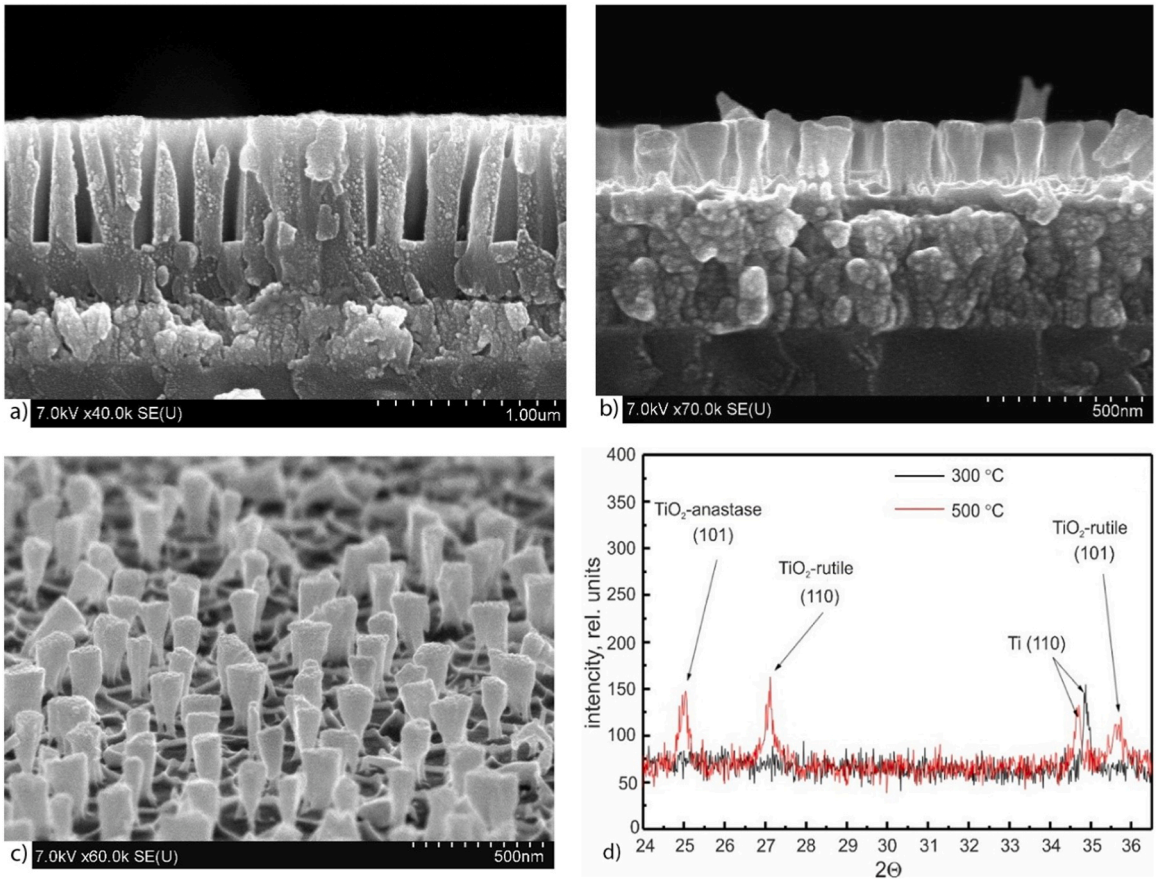

Fig. 1. The cross-section of AA matrix with titanium metal oxide columns into the pores (**a**); images of the titanium oxide columns after AA dissolution (**b**), (**c**); and X-ray diffraction patterns of the titanium oxide columns annealed at 300 °C and 500 °C (**d**).

The phase composition and microstructure of the formed films were determined based on the analysis of diffraction data obtained on the Bruker installation in CuK_α radiation (40 kV; 40 mA) at a wavelength of 1.54187 Å at room temperature in the range of 20.00 - 80.00 degrees with a scanning speed of 2°/min using databases ICDD PDF-2 Release 2013 and ICDD PDF-2 Release 2003, programs "FULLPROF" and "March! 3". During the research, the atomic structure of the films, the space group of the unit cell, its dimensions and shape, as well as the symmetry group of the crystal were determined.

The identification of chemical elements in the composition of the obtained films was determined using electron probe X-ray spectral microanalysis (EDX) using a Bruker QUANTAX 200 add-on with an XFlash silicon drift detector (SDD) with active area of 60 mm^2 for scanning electron microscope. Energy resolution <125 eV at Mn-K_α, detection from beryllium (Z = 4) to americium (Z = 95). The spot from the primary beam with energy of 15.4 keV had characteristic size of 2 μm and was directed into the cross section of the cleaved samples. The beam penetration depth ranged from 0.1 μm to several microns. The surface was excited at the site of accumulation of titanium oxide columns covered with bismuth oxide plates. When interpreting the spectra, the excitation zone was a drop-like region in micrometer-sized experimental sample.

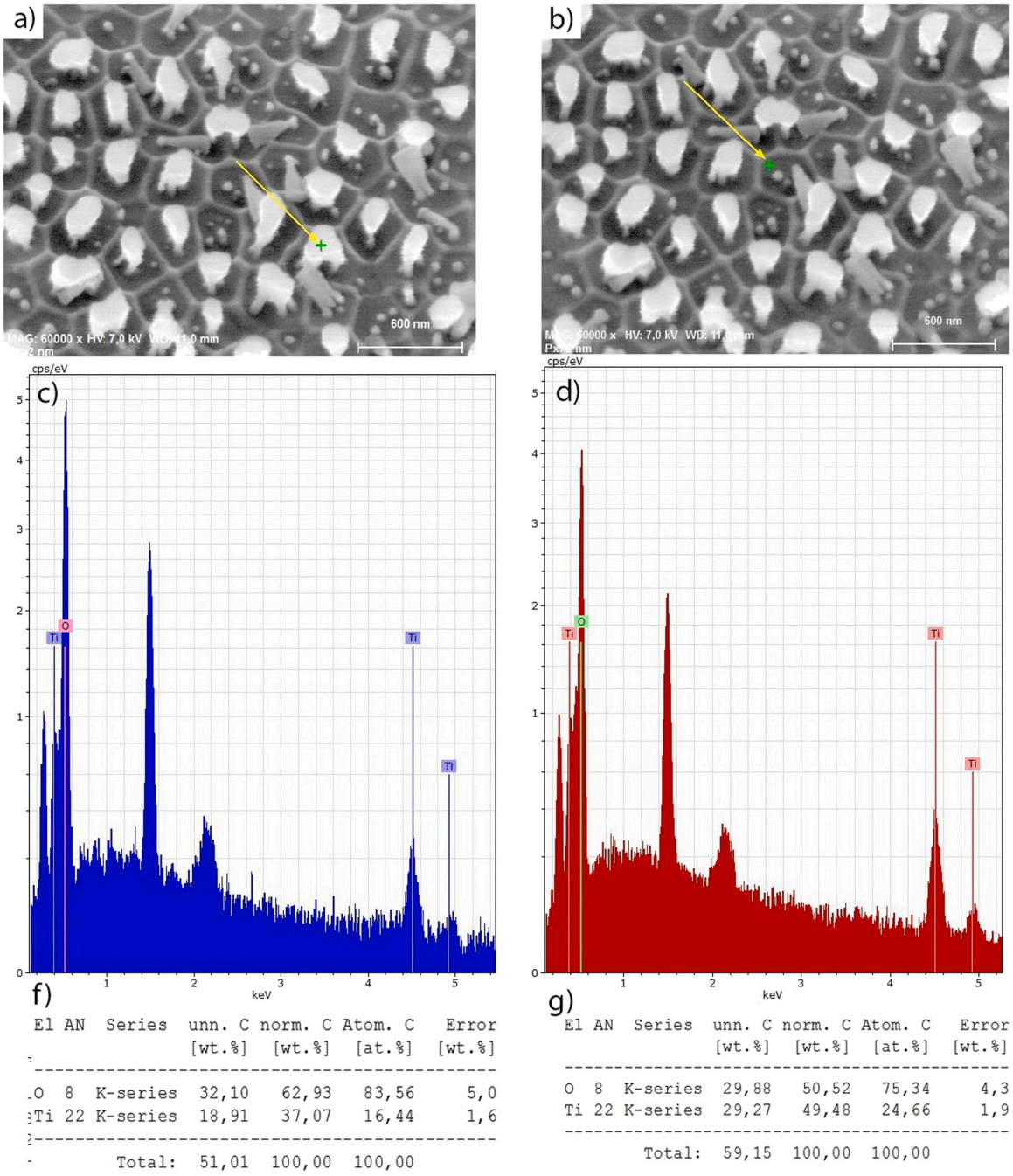

Fig. 2. The surfaces of the TiO_2 matrixes (arrows indicate the places where microanalysis was done), (**a**) – on columns and (**b**) – on intercolumn space; EDX spectrum of the TiO_2 oxide system (**c**) – on columns and (**c**) – on intercolumn space; and the tables of X-ray energy-dispersive microanalysis data (**f**) – on columns and (**g**) – on intercolumn space.

3. Results and discussion

3.1. Research of titanium metal oxide columns matrix

Fig. 1b–c shows the electron microscopic images of the titanium oxide columns after AA dissolution. The surface contains the accumulation of evenly spaced convex formations of various shapes with sizes from 140 to 160 nm, separated by gaps, the width of which is much less than the size of the columns. The number of columns corresponds to the number of pores in the AA. In this case, the total size of columns and spaces between them is approximately equal to the size of AA oxide cells. The columns height is 260 nm, and under the columns, there is a partially oxidized titanium layer [42]. Fig. 2a,b shows *SEM* image of array of titanium columns, the *EDX* spectrum of directly columns (Fig. 2c) and on intercolumn space(Fig. 2d), and also a table of electron probe X-ray energy-dispersive spectral microanalysis data (Fig. 2f,g). The *EDX* spectrum is shown contains of Ti and O. The elemental composition of the columns themselves and the space between the columns is the same, it consists only of titanium oxides, but the ratio of titanium and oxygen in the columns themselves is approximately one and a half times lower than between them. The atomic ratio of Ti and O for columns is 16.44 % and 83.56 %, and on intercolumns space– 24.66 % Ti and 75.34 %.

Previously discovered [41,43] that nanosized columns formed by electrochemical anodization of thin-film Ti/Al composition consist mainly of quasi-amorphous titanium dioxide in the form of anatase and rutile, with the presence of inclusions of other oxide modifications of Ti_2O_3 and TiO. Vacuum annealing, as shown using Auger electron spectroscopy [42], leads to the migration of oxygen from the outer part of the columns into the depths, as well as to its dissolution in the non-anodized titanium film. This leads to a noticeable decrease in oxygen at the tops of nanopillars and its increase in the volume of the film [42].

The microstructure of titanium oxide columns was studied by X-ray diffraction analysis. Fig. 1d shows the X-ray diffraction pattern of the columns annealed at 300 °C and 500 °C. The spectrum at 300 °C contains characteristic peaks for anatase with a trigonal crystal lattice with linear parameters $a = 5.126$ Å and $c = 13.8780$ Å [44], while unoxidized titanium is present in the film in the form of a metal nanomesh made of non-anodized titanium, placed along the boundary between AA oxide cells [42,43]. Metallic titanium remained in the gaps between the islands under the dense oxide film, which is appeared in the form of reflexes at $2\Theta = 34.4–34.8°$. After annealing at 500 °C, anatase predominantly transforms into rutile modification with tetragonal crystal system with linear parameters $a = 5.4600$ Å and $c = 32.8100$ Å [45]. The crystal space group was determined as *C*, consisting of crystalline phases (110) and (101), but the peaks from both anatase (101) and unoxidized titanium (110) are preserved in the diffraction pattern.

3.2. Surface morphology investigation of annealed TiO_2/Bi_2O_3 oxide system

After the deposition of bismuth oxide on titanium oxide columns, the film morphology acquired different form. Fig. 3a shows *SEM* image of annealed at 150 °C TiO_2/Bi_2O_3 sample surface and a table of electron probe X-ray energy-dispersive spectral microanalysis data, and the *EDX* spectrum itself is shown in Fig. 32b. The EDX spectrum contains all elements of the system under study, with Bi predominating. The atomic ratio of Bi, Ti and O, taking into account all the elements that make up the films, was 31.46 % Bi: 3.78 % Ti: 51.05 % O. Silicon and carbon identified in the composition of the obtained films belong to the silicon substrate and atmospheric carbon absorbed on the nanostructured surface.

Fig. 4a–h shows electron microscopic images of the surface and transverse cleavages of annealed composite films at temperatures of 150, 300, 500, and 700 °C. Based on the results of electron microscopic studies of the samples surface morphology, the configuration of the Bi_2O_3 plates, their geometric dimensions, mutual arrangement, and packing density were estimated. The Bi_2O_3 metal oxide located on the TiO_2 island film surface has the form of chaotically and vertically arranged plates, the horizontal dimensions of which vary in length in the range of 270–290 nm, and in width 35–40 nm. Between the plates, there are voids of various shapes, and the size of these voids is not the same over the entire surface of the film. At the same time, the pattern is observed — in areas with voids between the plates of larger size, the vertical size of the plates, and, accordingly, the thickness of the Bi_2O_3 film is greater, and vice versa, where the plates are denser, the height of the plates and the film thickness are smaller. Hence, it follows that the packing density of Bi_2O_3 plates over the substrate surface is not the same.

When comparing samples annealed at different temperatures, the following observations can be noted. The surface morphology of samples annealed at temperature of 150 °C practically does not differ from unannealed films (Fig. 4a,b). However, after annealing at 300 °C, some weakly noticeable morphological changes are already observed – densification of the Bi_2O_3 film and thickening of the TiO_2 film (Fig. 4c, d). In this case, the geometric dimensions of the Bi_2O_3 plates do not change. After annealing at 500 °C, significant changes were found in the

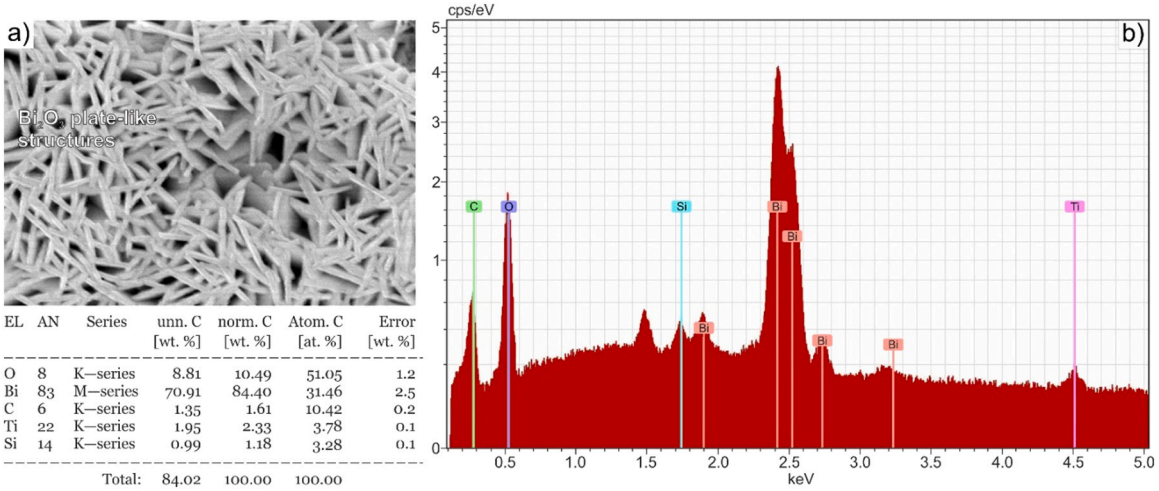

EL	AN	Series	unn. C [wt. %]	norm. C [wt. %]	Atom. C [at. %]	Error [wt. %]
O	8	K–series	8.81	10.49	51.05	1.2
Bi	83	M–series	70.91	84.40	31.46	2.5
C	6	K–series	1.35	1.61	10.42	0.2
Ti	22	K–series	1.95	2.33	3.78	0.1
Si	14	K–series	0.99	1.18	3.28	0.1
Total:			84.02	100.00	100.00	

Fig. 3. The surface of the TiO_2 matrix with the deposited Bi_2O_3 film annealed at 150 °C and the table of X-ray energy-dispersive microanalysis data (**a**); EDX spectrum of the Bi_2O_3/TiO_2 oxide system (**b**).

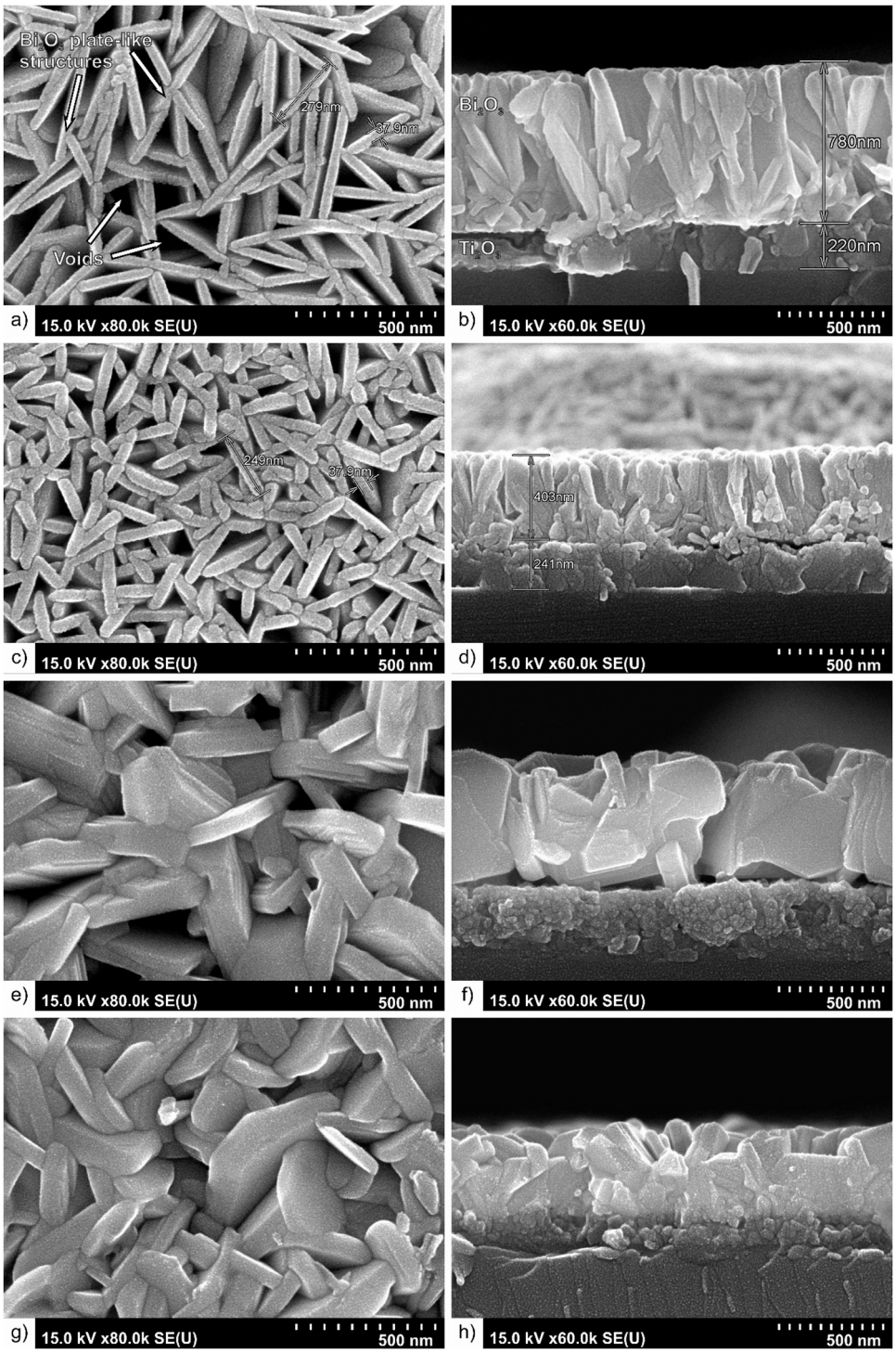

Fig. 4. SEM images of the surfaces (**a,c,e,j**) and cross-sections (**b,d,f,h**) of TiO_2 matrix with Bi_2O_3 film deposited on it, annealed at temperatures of 150 °C – (**a,b**); 300 °C – (**c,d**); 500 °C - (**e,f**) and 700 °C - (**g,h**) for 1.5 h.

structure of Bi_2O_3 (Fig. 4e,f). There was an enlargement of the geometric dimensions of the plates in length up to 390 – 420 nm, and in thickness up to 80 – 100 nm. At the same time, the thickness of the Bi_2O_3 film also increased to 650 nm and TiO_2 to 300 nm. A subsequent increase in the annealing temperature to 700 °C led to even more dramatic changes in the morphology of the Bi_2O_3/TiO_2 composite (Fig. 4g,h). The Bi_2O_3 plates, which previously had approximately the same dimensions, were transformed into grains with sizes from 200 to 600 nm; the voids between them decreased, and practically disappeared in the depth of the film. The thickness of the Bi_2O_3 film decreased to 430 nm and TiO_2 thickness — to 215 nm. The overall film thickness also decreased, and the boundary between the films became barely noticeable. Such morphological changes in the shape and size of metal oxide crystallites are probably caused by the transformation of the composite material microstructure as result of high-temperature annealing.

3.3. *X-ray structural analysis of annealed TiO_2/Bi_2O_3 oxide system*

Fig. 5 shows the diffraction patterns for samples annealed at temperatures of 150, 300, 500, and 700 °C. The diffraction pattern of the

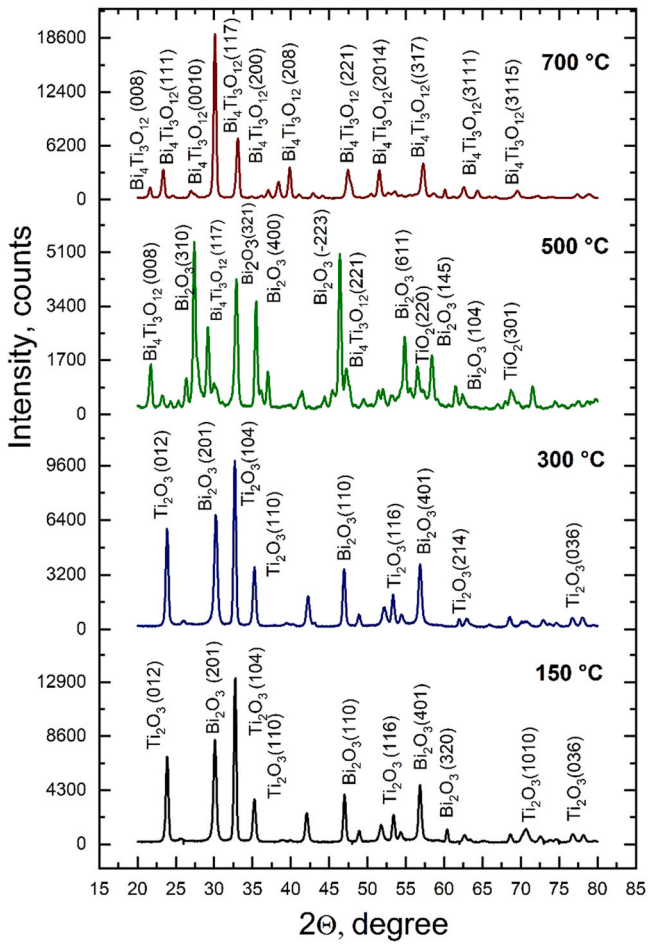

Fig. 5. X-ray diffraction pattern of TiO_2 matrix with Bi_2O_3 film deposited on it at annealing temperatures of 150, 300, 500, and 700 °C.

sample annealed at 150 °C contains peaks from Ti_2O_3 – (012) crystalline phases at 2Θ = 23.90°; (104) - 32.77°; (110) – 35.27°; (116) – 53.43° and (1010) – 70.70°. These experimental XRD patterns match well with the International Centre for Diffraction Data (ICDD) reference cards 01–071-1047. The spectrum also contains peaks (201) characteristic of Bi_2O_3 at 2Θ = 30.14°; (110) – 47.05°; (401) – 56.88°; and (320) – 60.42 in accordance with ICDD cards number 00–051-1161. The spectrum of the sample annealed at 300 °C practically remained unchanged, only the peaks of Bi_2O_3 (320) at 2Θ = 60.42° and Ti_2O_3 (1010) at 2Θ = 70.70° disappeared. At this stage, annealing leads to amorphization of titanium oxide in the composition of nanosized islands and to decrease in the relative content of the fraction of Ti_2O_3 and TiO inclusions in titanium dioxide. The changes that occur are the consequence of the dissolution of oxygen contained in the columnar structures in the bulk of the unanodized titanium layer [38].

After annealing at 500 °C (Fig. 5), not only morphological changes, but also significant transformations in the microstructure occurred in the studied composite. Titanium oxide passed into the rutile modification with peaks from the crystalline phases — (220) at 2Θ = 56.50° and (301) – 68.75°, which has a tetragonal crystalline system with linear parameters a = 5.4600 Å and c = 32.8100 Å in accordance with ICDD reference card number 00–034-0180.

In the volume of the film, the oxide phases Ti_2O_3 and Bi_2O_3 began to transform into the three-component compound $Bi_4Ti_3O_{12}$. This is evidenced by the new peaks on the diffraction pattern — (008) at 2Θ = 21.76°; (117) – 30.04°and (221) – 47.29 in accordance with ICDD cards number 00–047-0398. Bismuth titanate acquired the tetragonal crystal lattice with linear parameters a = 5.4600 Å and c = 32.8100 Å. The space group of the crystal was defined as *C*. The calculated density of the resulting $Bi_4Ti_3O_{12}$ was 7.956 g/cm^3. The main crystal lattice parameters characterizing the microstructure transformations and phase transformations of the Ti_2O_3 and Bi_2O_3 system are shown in Table 1.

The Bi_2O_3 phase appeared on the diffraction pattern at seven peaks, but the intensity of these peaks was not high, and they slightly shifted compared to the similar peaks found in the previous annealing stages. As a rule, the X-ray peak shift occurs for three reasons: the change in the lattice parameter, the presence of residual stresses, and the change in the concentration of defects. The shift of the Bragg peaks to higher values of the diffraction angle means decrease in the grating parameter. Several reasons are possible: elimination of defects, structural relaxation. The increasing in the intensity of the peaks with the increasing in the annealing temperature indicates the increased in the level of film crystallization [51].

After annealing at 700 °C (Fig. 5), the composite became single-phase. The diffraction pattern contains peaks from $Bi_4Ti_3O_{12}$ crystalline phases: (008) at 2Θ = 21.74°; (111) – 23.44°; (0010) – 27.07°; (117) – 30.20°; (200) – 33.18°; (208) – 39.95°; (221) – 47.54°; (2014) – 51.63°; (317) – 57.35°; (3111) – 62.66° and (3115) – 69.65 in accordance with ICDD cards number 00–012-0213. Bismuth titanate has an orthorhombic crystal lattice with linear parameters a = 5.4100 Å, b = 5.4480 Å, and c = 32.8400 Å.

Analyzing the phase transformations of the structure that occurred during annealing of the TiO_2/Bi_2O_3 oxide system during annealing from 150 to 700 °C, we can conclude that at temperatures up to 500 °C, no visible changes occur in the system under study. But already at 500 °C, microstructure transformations begin — TiO_2 from anatase it passes into the rutile phase, titanium is further oxidized, Bi_2O_3 begins to transform into bismuth titanate, and this process ends at 700 °C with the formation of the single-phase $Bi_4Ti_3O_{12}$ nanocomposite with orthorhombic crystal system of the *Fmmm* space group (see Table 1).

Thus, a combination of known methods made it possible to synthesize the composite important for practical use. In fact, this approach is a model for the synthesis of not only $Bi_4Ti_3O_{12}$, but also other compounds. In addition, the proposed technique differs from all known methods in its simplicity (no expensive equipment is required), low cost (we use weakly concentrated solutions of inexpensive chemicals), reproducibility of morphology and composition, controlled thickness and environmental friendliness.

4. Conclusions

An original technique for the formation of nanostructured bismuth titanate films based on electrochemical anodizing of Ti/Al thin-film system and SILD of bismuth oxide on the formed TiO_2 columns is proposed. The composition and morphology of the surface of the obtained oxide system after annealing in the temperature range 150–700 C were studied. After annealing to 300 °C, nanosized columns of titanium oxide consist mainly of quasi-amorphous dioxide in the form of anatase and rutile, with small amount of other oxide modifications Ti_2O_3 and TiO. The Bi_2O_3 metal oxide located on the TiO_2 columnar film surface has the form of chaotically and vertically arranged plates, the horizontal dimensions of which vary in length in the range of 270–290 nm, and in width 35–40 nm. The crystal system of the Bi_2O_3 phase is hexagonal with the crystal space group *P-3m1*. Between the plates, there are voids of various shapes, and the size of these voids is not the same over the entire surface of the film. After annealing at 500 °C, not only morphological changes occurred in the studied composite, but also significant transformations in the microstructure. Titanium oxide passed into the rutile modification with peaks from crystalline phases — (220) at 2Θ = 55.59° and (301) – 68.64°, which has the tetragonal crystal system. In the volume of the film, oxide phases Ti_2O_3 and Bi_2O_3 began to transform into the three-component compound $Bi_4Ti_3O_{12}$, and this process is completed at 700 degrees with the formation of single-phase $Bi_4Ti_3O_{12}$ nanocomposite with the orthorhombic crystal system *Fmmm* space

Table 1
Phase transformations upon annealing of the Ti_2O_3/Bi_2O_3 oxide system.

Temperature annealing, °C	Oxide phase	Crystal system	Linear parameters	Space group of crystal	Estimated Density
150	Ti_2O_3, anatase,[45]	Trigonal	$a = 5.126$ Å, $c = 13.878$ Å	*R-3c*	4536
	Bi_2O_3,[46]	Hexagonal	$a = 3.8780$ Å, $c = 6.3030$ Å	*P-3m1*	not determined
300	Ti_2O_3, anatase, rutile[46]	Trigonal	$a = 5.1251$ Å, $c = 13.957$ Å	*R-3c*	4512
	Bi_2O_3,[46]	Hexagonal	$a = 3.8780$ Å, $c = 6.3030$ Å	*P-3m1*	not determined
500	Bi_2O_3[47]	Monoclinic	a = 5.848 Å, b = 8.1660 Å, c = 7.5111 Å. β = 113	*P21/c*	9373
	TiO_2, rutile,[48]	Trigonal	a = 4.5930 Å c= 2.9590 Å	*P42/mnm*	4250
	$Bi_4Ti_3O_{12}$,[49]	tetragonal	a = 5.4600 Å, c = 32.810 Å.	*C*	7956
700	$Bi_4Ti_3O_{12}$,[50]	orthorhombic	a = 5.4100 Å, b = 5.4480 Å, c = 32.840 Å.	*Fmmm*	8.11

group.

Declaration of Competing Interest

The authors declare that they have no known competing financial interests or personal relationships that could have appeared to influence the work reported in this paper.

References

[1] B.H. Park, B.S. Kang, S.D. Bu, T.W. Noh, J. Lee, W. Jo, Lanthanum-substituted bismuth titanate for use in non-volatile memories, Nature 401 (1999) 682–684, https://doi.org/10.1038/44352.

[2] U. Chon, H.M. Jang, M.G. Kim, C.H. Chang, Layered perovskites with giant spontaneous polarizations for nonvolatile memories, Phys. Rev. Lett. 89 (2002) 087601, https://doi.org/10.1103/PhysRevLett.89.087601.

[3] Y. Zhang, W. Jie, P. Chen, W. Liu, J. Hao, Ferroelectric and piezoelectric effects on the optical process in advanced materials and devices, Adv. Mater. 30 (2018) 1707007, https://doi.org/10.1002/adma.201707007.

[4] N.A. Spaldin, Magnetic Materials: Fundamentals and Applications, Cambridge University Press,, Cambridge, 2010, https://doi.org/10.1017/CBO9780511781599.

[5] U.I. Gaya, A.H. Abdullah, Heterogeneous photocatalytic degradation of organic contaminants over titanium dioxide: a review of fundamentals, progress and problems, J. Photochem. Photobiol. C: Photochem. Rev. 9 (2008) 1–12, https://doi.org/10.1016/j.jphotochemrev.2007.12.003.

[6] M.N. Chong, B. Jin, C.W.K. Chow, C. Saint, Recent developments in photocatalytic water treatment technology: a review, Water Res. 44 (2010) 2997–3027, https://doi.org/10.1016/j.watres.2010.02.039.

[7] F. Han, V.S.R. Kambala, M. Srinivasan, D. Rajarathnam, R. Naidu, Tailored titanium dioxide photocatalysts for the degradation of organic dyes in wastewater treatment: a review, Appl. Catal. A: Gen. 359 (2009) 25–40, https://doi.org/10.1016/j.apcata.2009.02.043.

[8] S. Feizpoor, A. Habibi-Yangjeh, S. Vadivel, Novel TiO2/Ag2CrO4 nanocomposites: efficient visible-light-driven photocatalysts with n–n heterojunctions, J. Photochem. Photobiol. A: Chem. 341 (2017) 57–68, https://doi.org/10.1016/j.jphotochem.2017.03.028.

[9] L. Di, H. Yang, T. Xian, X. Chen, Enhanced photocatalytic activity of NaBH4 reduced BiFeO3 nanoparticles for rhodamine B decolorization, Mater. (Basel) 10 (2017) 1118, https://doi.org/10.3390/ma10101118.

[10] X. Tong, Y. Zhou, L. Jin, K. Basu, R. Adhikari, G.S. Selopal, X. Tong, H. Zhao, S. Sun, A. Vomiero, Z.M. Wang, F. Rosei, Heavy metal-free, near-infrared colloidal quantum dots for efficient photoelectrochemical hydrogen generation, Nano Energy 31 (2017) 441–449, https://doi.org/10.1016/j.nanoen.2016.11.053.

[11] X. Tong, X.-T. Kong, Y. Zhou, F. Navarro-Pardo, G.S. Selopal, S. Sun, A.O. Govorov, H. Zhao, Z.M. Wang, F. Rosei, Near-infrared, heavy metal-free colloidal "Giant" core/shell quantum dots, Adv. Energy Mater. 8 (2018) 1701432, https://doi.org/10.1002/aenm.201701432.

[12] H. Zhang, M. Lü, S. Liu, L. Wang, Z. Xiu, Y. Zhou, Z. Qiu, A. Zhang, Q. Ma, Preparation and photocatalytic property of perovskite Bi4Ti3O12 films, Mater. Chem. Phys. 114 (2009) 716–721, https://doi.org/10.1016/j.matchemphys.2008.10.052.

[13] X. Lin, Q.-F. GUAN, T.-T. LIU, Y. ZHANG, C.-J. ZOU, Controllable synthesis and photocatalytic activity of Bi4Ti3O12 particles with different morphologies, Acta Phys. -Chim. Sin. 29 (2013), https://doi.org/10.3866/PKU.WHXB201211211.

[14] H. He, J. Yin, Y. Li, Y. Zhang, H. Qiu, J. Xu, T. Xu, C. Wang, Size controllable synthesis of single-crystal ferroelectric Bi4Ti3O12 nanosheet dominated with {001} facets toward enhanced visible-light-driven photocatalytic activities, Appl. Catal. B: Environ. 156–157 (2014) 35–43, https://doi.org/10.1016/j.apcatb.2014.03.003.

[15] Z. Chen, H. Jiang, W. Jin, C. Shi, Enhanced photocatalytic performance over Bi4Ti3O12 nanosheets with controllable size and exposed {001} facets for Rhodamine B degradation, Appl. Catal. B: Environ. 180 (2016) 698–706, https://doi.org/10.1016/j.apcatb.2015.07.022.

[16] K. Qian, Z. Jiang, H. Shi, W. Wei, C. Zhu, J. Xie, Constructing mesoporous Bi4Ti3O12 with enhanced visible light photocatalytic activity, Mater. Lett. 183 (2016) 303–306, https://doi.org/10.1016/j.matlet.2016.07.121.

[17] Yu.A. Vashpanov, V.A. Smyntyna, Adsorption sensitivity of semiconductors Odessa: Astroprint, 2005. - 190 p.

[18] T. Wolkenstein, Electronic Processes on Semiconductor Surfaces during Chemisorption, 1991st edition, Springer, New York, 1991.

[19] Y. Deng, Semiconducting Metal Oxides for Gas Sensing, Springer Nature Singapore,, 2023.

[20] A. Dey, Semiconductor metal oxide gas sensors: a review, Mater. Sci. Eng.: B 229 (2018) 206–217, https://doi.org/10.1016/j.mseb.2017.12.036.

[21] A. Ponzoni, C. Baratto, N. Cattabiani, M. Falasconi, V. Galstyan, E. Nunez-Carmona, F. Rigoni, V. Sberveglieri, G. Zambotti, D. Zappa, Metal oxide gas sensors, a survey of selectivity issues addressed at the SENSOR lab, Brescia (Italy), Sensors 17 (2017) 714, https://doi.org/10.3390/s17040714.

[22] L. Obvintseva, Metal oxide semiconductor sensors for determination of reactive gas impurities in air, Russ. J. Gen. Chem. 78 (2008) 2545–2555, https://doi.org/10.1134/S1070363208120347.

[23] M.N. Rumyantseva, V.V. Kovalenko, A.M. Gas'kov, T. Pagnier, Metal-oxide based nanocomposites as materials for gas sensors, Russ. J. Gen. Chem. 78 (2008) 1081–1092, https://doi.org/10.1134/S1070363208050411.

[24] W. Zhao, Z. Jia, E. Lei, L. Wang, Z. Li, Y. Dai, Photocatalytic degradation efficacy of Bi4Ti3O12 micro-scale platelets over methylene blue under visible light, J. Phys. Chem. Solids 74 (2013) 1604–1607, https://doi.org/10.1016/j.jpcs.2013.06.003.

[25] C. Liu, J. Liang, R. Han, Y. Wang, J. Zhao, Q. Huang, J. Chen, W. Hou, S-doped Na2Ti6O13@TiO2 core–shell nanorods with enhanced visible light photocatalytic performance, Phys. Chem. Chem. Phys. 17 (2015) 15165–15172, https://doi.org/10.1039/C5CP01552A.

[26] Y. Shimizu, M. Egashira, Basic aspects and challenges of semiconductor gas sensors, MRS Bull. 24 (1999) 18–24, https://doi.org/10.1557/S0883769400052465.

[27] I.V. Roslyakov, K.S. Napolskii, V.S. Stolyarov, E.E. Karpov, A.V. Ivashev, V. N. Surtaev, A thin-film platform for chemical gas sensors, Russ. Micro 47 (2018) 226–233, https://doi.org/10.1134/S1063739718040078.

[28] G. Gorokh, A. Zakhlebayeva, A. Lazavenka, N. Sobolev, V. Zhylinski, N. Bogomazova, M. Yarmolich, N. Kalanda, Functional multicomponent metal oxide films based on Sr, Sn, Fe, and Mo in the anodic alumina matrices, Phys. Status Solidi (B) 257 (2020) 1900283, https://doi.org/10.1002/pssb.201900283.

[29] A. Zakhlebayeva, A. Lazavenka, G. Gorokh, Multicomponent Sn–Mo–O-containing films formed in anodic alumina matrixes by ionic layer deposition, Mater. Today: Proc. 37 (2021) 4064–4070, https://doi.org/10.1016/j.matpr.2020.09.252.

[30] V. Khatko, A. Mozalev, G. Gorokh, D. Solovei, F. Gispert Guirado, E. Llobet, X. Correig, Evolution of surface morphology and crystal texture of WO3 layers sputtered onto Si-supported nanoporous alumina templates, K116–K123, J. Electrochem. Soc. 155 (2008), https://doi.org/10.1149/1.2918902.

[31] G.G. Gorokh, M.I. Pashechko, J.T. Borc, A.A. Lozovenko, I.A. Kashko, A.I. Latos, Matrix coatings based on anodic alumina with carbon nanostructures in the pores, Appl. Surf. Sci. 433 (2018) 829–835, https://doi.org/10.1016/j.apsusc.2017.10.117.

[32] A. Zakhlebayeva, G. Gorokh, A. Lazavenka, Nanostructured Composite Films Based on Oxides of Tin, Molyb-denum, Nickel in Porous Matrices of Anodic Alumina. In: Nanostructured oxide films and coatings, ed.: N.M. Yakovleva; PetrSU; Petrozavodsk, 2021; 189–200. ISBN 978–5-8021–3849-6.

[33] G. Gorokh, I. Obukhov, A. Lazavenka, Indium antimonide nanowires arrays for promising thermoelectric converters, "Tekhnologiya i Konstruirovanie v Elektronnoi Apparature" ("Technology and Design in Electronic Equipment") ISSN 2225–5818. 2015 (2015) 3–12. https://doi.org/10.15222/TKEA2015.1.03.

[34] G.G. Gorokh, A.I. Zakhlebayeva, A.I. Metla, V.V. Zhilinskiy, A.N. Murashkevich, N. V. Bogomazova, Formation of multicomponent matrix metal oxide films in anodic alumina matrixes by chemical deposition, J. Phys.: Conf. Ser. 917 (2017) 092011, https://doi.org/10.1088/1742-6596/917/9/092011.

[35] G. Korotcenkov, B.K. Cho, L.B. Gulina, V.P. Tolstoy, Gas sensor application of Ag nanoclusters synthesized by SILD method, Sens. Actuators B: Chem. 166–167 (2012) 402–410, https://doi.org/10.1016/j.snb.2012.02.081.

[36] V. Tolstoy, S. Han, G. Korotcenkov, Successive Ionic Layer Deposition (SILD): Advanced Method for Deposition and Modification of Functional Nanostructured Metal Oxides Aimed for Gas Sensor Applications, in: 2010: pp. 384–436. https://doi.org/10.13140/2.1.2131.2648.
[37] L.B. Gulina, V.P. Tolstoy, The synthesis by successive ionic layer deposition of SnMo0.6Oy·nH2O nanolayers on silica, Thin Solid Films 440 (2003) 74–77, https://doi.org/10.1016/S0040-6090(03)00684-9.
[38] A. Mozalev, G. Gorokh, M. Sakairi, H. Takahashi, The growth and electrical transport properties of self-organized metal/oxide nanostructures formed by anodizing Ta-Al thin-film bilayers, J. Mater. Sci. 40 (2005) 6399–6407, https://doi.org/10.1007/s10853-005-1620-9.
[39] V. Surganov, G. Gorokh, Array of Niobium Nanotips Formed in Porous Anodic Alumina Matrix, Proceedings of SPIE - The International Society for Optical Engineering. (2000). https://doi.org/10.1117/12.382321.
[40] A. Mozalev, M. Sakairi, H. Takahashi, Structure, morphology, and dielectric properties of nanocomposite oxide films formed by anodizing of sputter-deposited Ta-Al bilayers, J. Electrochem. Soc. 151 (11) (2004) F257, https://doi.org/10.1149/1.1796445.
[41] V.F. Surganov, A.M. Mozalev, V.A. Lastochkina, Investigating the composition of periodic nano-size column structures of anodic titanium oxide by the method of IR spectroscopy, J. Appl. Spectrosc. 65 (1998) 891–897, https://doi.org/10.1007/BF02675745.
[42] N.I. Tatarenko, A.M. Mozalev, Geometry and element composition of a nanoscale field emission array formed by self-organization in porous anodic aluminum oxide, Solid-State Electron. 45 (6) (2001) 1009–1016, https://doi.org/10.1016/s0038-1101(01)00022-3.
[43] V.F. Surganov, A.M. Mozalev, N.I. Tatarenko, V.A. Lastochkina, IR spectroscopic studies of periodic columnar nanostructures of anodic titanium oxide, J. Appl. Spectrosc. 65 (2) (1998) 206–210, https://doi.org/10.1007/bf02680470.
[44] Ref. from ICSD using POWD-12++ 11, 1355 (1997).
[45] A.L. Castro, M.R. Nunes, A.P. Carvalho, F.M. Costa, M.H. Florêncio, Synthesis of anatase TiO2 nanoparticles with high temperature stability and photocatalytic activity, Solid State Sci. 10 (2008) 602–606, https://doi.org/10.1016/j.solidstatesciences.2007.10.012.
[46] T. Atou, H. Faqir, M. Kikuchi, H. Chiba, Y. Syono, A new high-pressure phase of bismuth oxide, Mater. Res. Bull. 33 (1998) 289–292, https://doi.org/10.1016/S0025-5408(97)00216-X.
[47] Medernach, J., Snyder, N.Y.S. College of Ceramics, Alfred Univ., Alfred, New York, USA, ICDD Grant-in-Aid.
[48] Smith, Zolensky, Dept. Geol. Sciences, Penn State Univ., University Park, PA, USA, ICDD Grant-in-Aid (1979).
[49] O. Yamaguchi, N. Maruyama, K. Hirota, The formation and characterization of alkoxy-derived Bi4Ti3O12, Br. Ceram., Trans. J. 90 (1991) 111–113.
[50] K. Momma, F. Izumi, VESTA 3 for three-dimensional visualization of crystal, volumetric and morphology data, J. Appl. Crystallogr. 44 (2011), https://doi.org/10.1107/S0021889811038970.
[51] D.L. Freimund, H. Batelaan, Bragg scattering of free electrons using the Kapitza-Dirac effect, Phys. Rev. Lett. 89 (2002) 283602, https://doi.org/10.1103/PhysRevLett.89.283602.